RSC Advances

ROYAL SOCIETY OF CHEMISTRY

www.rsc.org/advances

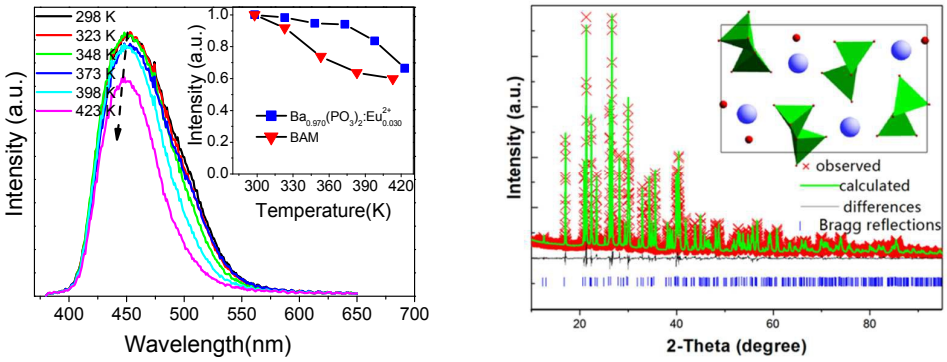

The luminescence of $Ba_{0.970}(PO_3)_2$: $Eu^{2+}_{0.030}$ shows higher thermal stability than that of commercial blue phosphor BAM.

Synthesis, crystal structure and photoluminescence properties of new blue-green $Ba_{1-x}(PO_3)_2$: Eu^{2+}_x ($0 < x \leq 0.040$) phosphors for near ultraviolet based white light-emitting diodes

Zhan-Chao Wu, *[a] Hong-Hong Fu, [a] Jie Liu, [a] Shao-Ping Kuang,[a] Ming-Mei Wu, *[b] Jun-Gu Xu[b, c] and Xiao-Jun Kuang[c]

a. *Key Laboratory of Sensor Analysis of Tumor Marker, Ministry of Education, Laboratory of Inorganic Synthesis and Applied Chemistry, College of Chemistry and Molecular Engineering, Qingdao University of Science and Technology, Qingdao 266042, P. R. China*

b. *School of Chemistry and Chemical Engineering, Sun Yat-Sen University, Guangzhou 510275, China*

c. *College of Materials Science and Engineering, Guilin University of Technology, Guilin 541004, P. R. China*

* Corresponding authors. Tel: +86 15806594068

E-mail address: wuzhan_chao@163.com (Zhan-Chao Wu), ceswmm@sysu.edu.cn (Ming-Mei Wu)

Abstract:

A series of new blue-green $Ba_{1-x}(PO_3)_2$: Eu^{2+}_x (x = 0.005, 0.010, 0.020, 0.030, 0.035, 0.040) phosphors were synthesized by solid state reaction. The phase purity and crystal structure were characterized by X-ray diffraction (XRD) and the Rietveld refinements. The photoluminescence properties were investigated by means of excitation, emission spectra and Commission International de L'Eclairage (CIE) chromaticity coordinates. Concentration quenching mechanism of Eu^{2+} emission in $Ba(PO_3)_2$ host was studied. The thermal stability was evaluated by temperature-dependent luminescence of $Ba_{0.970}(PO_3)_2$: $Eu^{2+}_{0.030}$ phosphor. Also, the activation energy (Ea) for thermal quenching was calculated. The photoluminescence of $Ba_{0.970}(PO_3)_2$: $Eu^{2+}_{0.030}$ phosphor shows higher thermal stability than that of commercial blue phosphor $BaMgAl_{10}O_{17}$: Eu^{2+} (BAM). All the results show that $Ba(PO_3)_2$: Eu^{2+} phosphor is an potential blue-green phosphor for near ultraviolet based white light-emitting diodes (WLED).

***Key words*:** Blue-green phosphor; Photoluminescence; White light-emitting diodes (WLED); Temperature-dependent luminescence; Phosphate

1. Introduction

White light emitting diodes (WLEDs) give a revolution on the illumination to replace conventional incandescent or fluorescence lamps in recent years due to their predominant superiority of high energy efficiency, long lifetime, and environmental friendliness.[1-3] At present, the $Y_3Al_5O_{12}:Ce^{3+}$ phosphor combined with blue InGaN chip is frequently used to create white light.[4-5] However, this method would suffer the challenge of low color rendering index (Ra < 80) and high correlated color temperature (Tc > 4500K) for lacking red component.[6] To obtain white light with high Ra and suitable Tc, another approach is the use of near-ultraviolet (NUV, 350-420 nm) LED chips with red, blue and green muti-phased phosphors.[7] In this case, it is an essential prospect to develop new phosphors which can be effectively excited by NUV chips.

As is well known, rare earth ions with rich energy levels have great agility in designing new luminescent materials.[8] Especially, Eu^{2+} is one of the most excellent activators due to its unique electronic configurations. Eu^{2+} has the $4f^7$ electronic configuration of the ground state and the $4f^65d^1$ electronic configuration of the excited state. Since the transition between $4f^7$ and $4f^65d^1$ states is spin and parity allowed, the absorption and emission of Eu^{2+} ions are broadband. In addition, the emission of Eu^{2+} ions strongly depends on the crystal field influenced by the nature of host and the ligand-activator interaction. When Eu^{2+} is incorporated into different compounds, different kinds of emission centers can be formed. So the color of the Eu^{2+} emission can vary from ultraviolet to red by selecting the appropriate host materials.[9-10]

As the phosphor-conversion (pc) luminescent materials applied in WLEDs, the phosphors are generally required to have high fluorescence conversion efficiency for NUV light, appropriate excitation and emission bands, as well as high chemical stability. In addition, they are desired to provide excellent thermally stable luminescence to withstand the high temperature generated by LEDs, which generally work at about 120 ^{o}C. The thermal stability of the phosphors influences greatly on the light output of pc-LEDs and lifetime of LEDs device. Meanwhile, the optimal blue phosphors are expected to be prepared at low temperature by cheap raw materials, considering that the high sintering temperature (over 1400 ^{o}C) of the commercial blue phosphor $BaMgAl_{10}O_{17}$: Eu^{2+} (BAM) is strict in production equipment and need to consume huge amounts of electric energy. Phosphors based on phosphates show many advantages such as low preparation temperature, high luminescence efficiency, cheap raw materials and relative stability of physical and chemical quality, compared with other host systems including aluminates ($SrAl_2O_4$:Eu^{2+}),[11] silicates (β-$Ca_3SiO_4Cl_2$: Eu^{2+}),[12] and nitrides ($(Sr,Ca)_2Si_5N_8$: Eu^{2+}),[13] et al.

In 1968, Costas C. Lagos reported on the UV excitation of the divalent europium activated $Ba(PO_3)_2$ at the earliest, which showed a weak violet emission band peaked at 375 nm under 253.7 nm exvitation.[14, 15] However, the structure of $Ba(PO_3)_2$: Eu^{2+} phosphor was not reported. Obviously, $Ba(PO_3)_2$: Eu^{2+} phosphor reported by Lagos can not be applied in WLEDs. Thereafter, there were few reports about it.

In this work, a series of new Eu^{2+}-activated blue-green phosphate phosphors $Ba_{1-x}(PO_3)_2$: Eu^{2+}_x (x = 0.005, 0.010, 0.020, 0.030, 0.035, 0.040) were prepared by

solid-state method at a lower temperature of 600 ^{o}C. Crystal structure, luminescence properties, and thermal stabilities of the phosphor were also investigated in detail. Finally, the activation energies (*E*a) for thermal quenching was calculated from the temperature-dependent luminescence of $Ba_{0.970}(PO_3)_2$: $Eu^{2+}_{0.030}$ phosphor.

2. Experimental section

2.1. Materials and synthesis

The $Ba_{1-x}(PO_3)_2$: Eu^{2+}_x samples (x = 0.005, 0.010, 0.020, 0.030, 0.035, 0.040) were synthesized by a solid-state reaction. The raw materials $BaCO_3$ (AR grade), $NH_4H_2PO_4$ (AR grade) and Eu_2O_3 (99.99% purity) were stoichiometrically weighed and thoroughly mixed by grinding in an agate mortar. Then they were put into alundum crucible and heated in muff furnace at 600 ^{o}C for 6 h in CO atmosphere. Finally, the synthesized samples were cooled to room temperature naturally for further experiment.

2.2. Measurements and characterization.

Crystal phase identification was carried out on an X-ray diffractometer (XRD, D-MAX2500/PC, RIGAKU Corporation, Japan) using 40 kV, 20 mA and Cu *K*α radiation (λ= 1.5418 Å). Microtopography and composition of the calcined particles were observed by scanning electron microscopy (SEM, JSM-6700F, JEOL, Japan) and energy disperse spectroscopy (EDS, INCA Energy, Oxford). Room temperature excitation and emission spectra of $Ba(PO_3)_2$: Eu^{2+} were analyzed by a fluorescence spectrophotometer (F-2700, HITACHI High-Technologies Corporation, Japan) with a photomultiplier tube operating at 400V, and a 150W Xe lamp was used as the

excitation source. Temperature-dependent luminescence was measured by a fluoromax-4 spectrofluorometer (HORIBA, JOBIN YVON, France) and the excitation sources used include a 150 W xenon lamp.

3. Results and discussion

3.1 Crystal structure and microtopography

The XRD patterns of $Ba_{1-x}(PO_3)_2$: Eu^{2+}_x samples (x = 0.005, 0.010, 0.020, 0.030, 0.035, 0.040) are shown in Fig. 1 and the standard data for $Ba(PO_3)_2$ (PDF card No.43-0518) are also shown as a reference. It shows that all the diffraction peaks of the samples can be well indexed to the standard data of PDF#43-0518, which has been refined to be orthorhombic with space group of $P2_12_12_1$ and cell parameters of a =4.499 Å, b = 13.394 Å, c = 8.340 Å, Z = 4 and V = 502.53 Å^3. The results indicate that the prepared phosphors are isostructural with $Ba(PO_3)_2$ and doping a little amount of Eu^{2+} has no obvious influence on the host structure. Also, no impurities are detected in the prepared products, suggesting that Eu^{2+} ions have been successfully incorporated in $Ba(PO_3)_2$ host lattice due to similar ionic radii and same valences of Ba^{2+} and Eu^{2+}.

To further study the structure of the obtained samples, Rietveld structure refinement of $Ba_{0.980}(PO_3)_2$: $Eu^{2+}_{0.020}$ phosphor was performed using Topas Academic software.[16] Figure 2 shows the observed, calculated and difference synchrotron XRD profiles for the Rietveld refinement of $Ba_{0.980}(PO_3)_2$: $Eu^{2+}_{0.020}$ phosphor. The results of the Rietveld refinement can further indicate that Ba^{2+} was substituted by Eu^{2+} ion in $Ba(PO_3)_2$ host and the incorporated Eu^{2+} ions caused no obvious impurity or

secondary phases. The lattice parameters of $Ba_{0.980}(PO_3)_2$: $Eu^{2+}_{0.020}$ phosphor are a = 4.50128(5) Å, b = 13.4005(1) Å, c = 8.34468(8) Å and V = 503.350(9) Å^3, which are changed slightly when doping a small amount of Eu^{2+} to replace Ba^{2+}. The final refined structural parameters are listed in Table 1. The refinement finally converged to R_p (Profile R value) = 3.60%, R_{wp} (Weighted-profile R value) = 4.82% and R_B (Bragg-intensity R value) = 2.07%, indicating all these factors satisfy well with the reflection condition. Fig. 3 and Fig. 4 show the refined unit cell structure of the samples. The Ba/Eu atoms, oxygen atoms and PO_4 tetrahedral are ploted in blue, red and green, respectively. The black numbers in Fig. 4 denote the interatomic distances between Ba/Eu and the coordinated O atom. In $Ba(PO_3)_2$ host, there is only one kind of Ba^{2+} site and Ba is defined as 10-coordinated. From the refinement results, the average length of Ba-O was calculated to be about 2.89 Å.

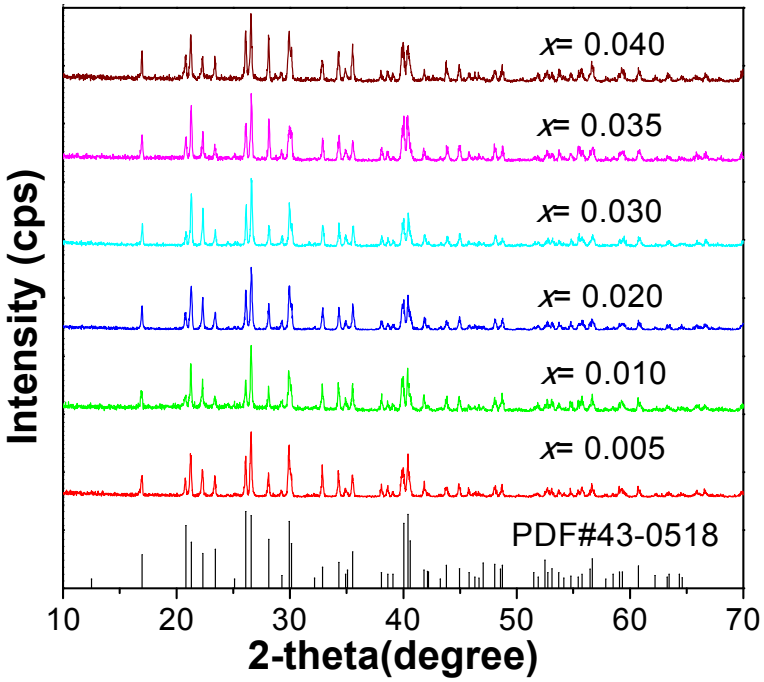

Fig. 1 XRD patterns of $Ba_{1-x}(PO_3)_2$: Eu^{2+}_x samples.

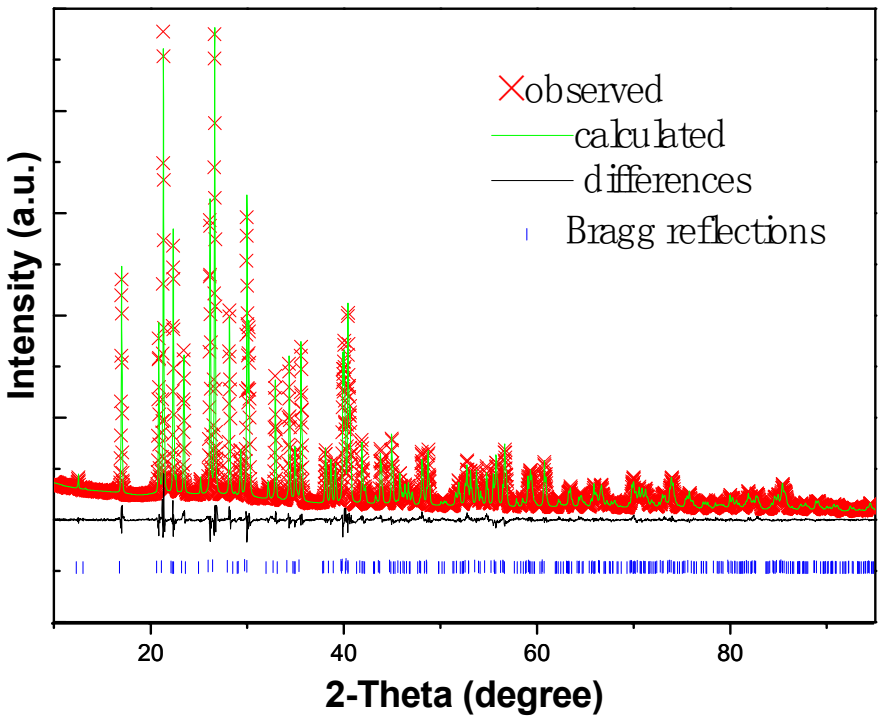

Fig 2. Rietveld plot of XRD data for $Ba_{0.980}(PO_3)_2$: $Eu^{2+}_{0.020}$

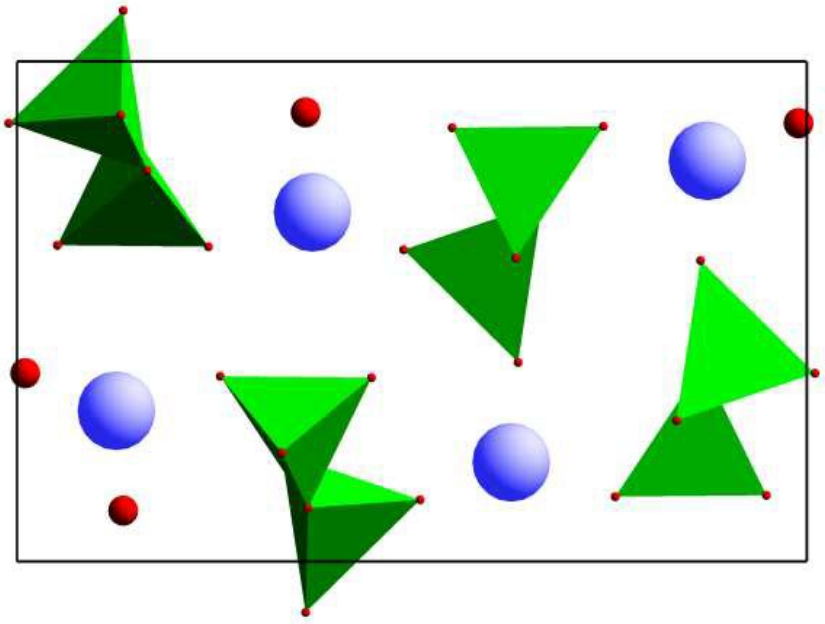

Fig. 3 Final refined unit cell $Ba_{0.980}(PO_3)_2$: $Eu^{2+}_{0.020}$

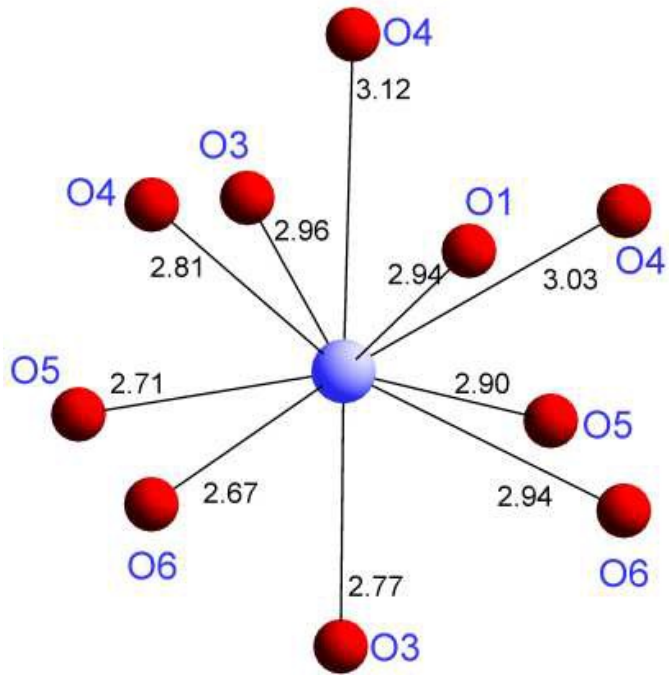

Fig. 4 The coordination state of Ba/Eu in $Ba_{0.980}(PO_3)_2$: $Eu^{2+}_{0.020}$.

Table 1 Final refined structural parameters of $Ba_{0.980}(PO_3)_2$: $Eu^{2+}_{0.020}$ phosphor

Atoms	x	y	z	Occup.	B_{iso} (Å^2)
Ba1	0.25899	0.12586	0.19855	0.98120	0.93568
Eu1	0.25899	0.12586	0.19855	0.01880	0.93568
P1	0.70993	0.35414	0.21916	1	1.00402
P2	0.21378	0.40271	0.42374	1	1.00402
O1	0.37794	0.33489	0.28201	1	0.47143
O2	0.88652	0.36844	0.39288	1	0.47143
O3	0.68331	0.44888	0.13245	1	0.47143
O4	0.79082	0.25747	0.12960	1	0.47143
O5	0.78578	0.01036	0.12345	1	0.47143
O6	0.79746	0.13454	0.39819	1	0.47143

a= 4.501 Å, b=13.401 Å, c=8.344 Å, V=503.350 Å^3, α=90º, β=90º, γ=90º, Z=4 with space group $P2_12_12_1$, R_p=3.60%, R_{wp}=4.82%, R_B=2.07%.

The morphology of $Ba_{0.970}(PO_3)_2$: $Eu^{2+}_{0.030}$ phosphor was observed by SEM (Fig. 5a). The microstructure of the phosphor consists of irregular fine grains with the diameters ranging from 200 - 300 nm. It seems that the surface of the particles is not smooth and every particle is composed of lots of tiny particles. So, the average crystalline size of the particles was estimated by the Debye-Scherrer equation:[17]

$$D = 0.89\,\lambda / \beta \cos(\theta) \qquad (1)$$

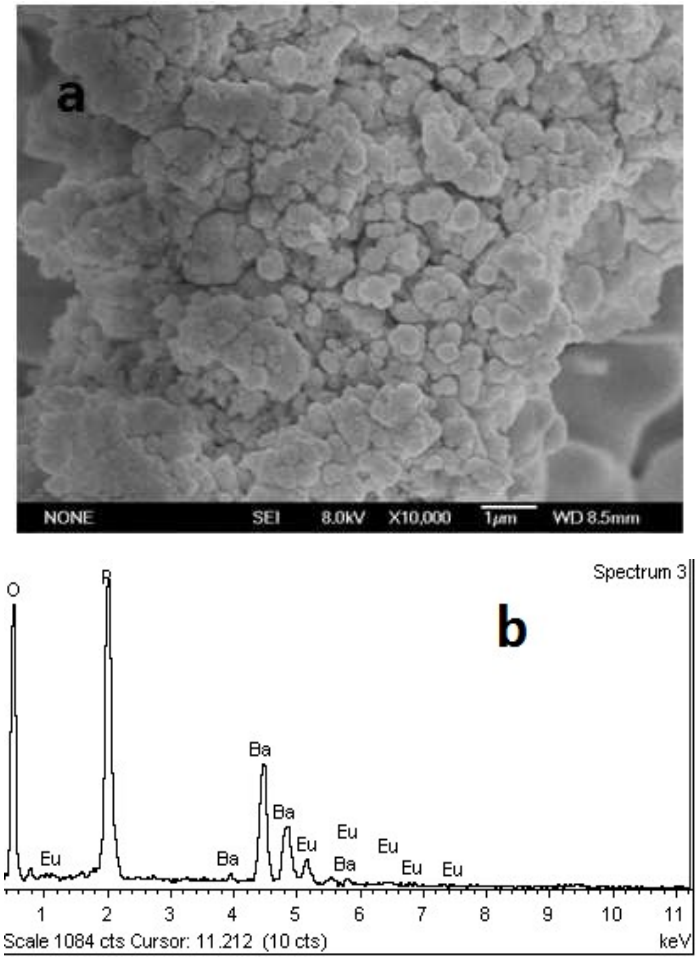

Fig. 5 (a) SEM image of $Ba_{0.970}(PO_3)_2$: $Eu^{2+}_{0.030}$ phosphor and (b) EDS of $Ba_{0.970}(PO_3)_2$: $Eu^{2+}_{0.030}$.

Where D is the average diameter of the particles, λ is the wavelength of the X-rays (1.5406 Å), β is the full-width in radiation at half-maximum (FWHM) of the peak, here $\beta = 0.06$, and θ is the Bragg angle of the X-ray diffraction peak. The calculated

crystal size of the phosphor is about 23 nm. These results show that lots of primary crystals reunite to agglomerates. The energy dispersive spectrum (EDS) of $Ba_{0.970}(PO_3)_2$: $Eu^{2+}_{0.030}$ shown in Fig. 5(b) reveals the major chemical elements (wt %) of Ba (43.22%), P (18.14%), O (30.43%) and Eu^{2+} (1.89%) in the host, which is basically conformed with the stoichiometric weight ratio of each element in $Ba_{0.970}(PO_3)_2$: $Eu^{2+}_{0.030}$ (Ba 45.03%, P 20.96%, O 32.46%, Eu^{2+} 1.5%).

3.2 Photoluminescence properties

Fig. 6 depicts the excitation and emission spectra of $Ba_{1-x}(PO_3)_2$: Eu^{2+}_x (x = 0.005, 0.010, 0.020, 0.030, 0.035, 0.040) phosphors at room temperature. Monitored at 445 nm, the samples show a broad intense excitation band from 220–400 nm, which matches with the emission of NUV chips. The excitation band mainly consists of three peaks located at 268, 323 and 350 nm, respectively. Since absorption bands of phosphate hosts are located in the vacuum ultraviolet region (100–200 nm),[18] the excitation bands in the range of 220–400 nm are attributed to the electronic transition from $4f^7$ ground state to $4f^65d^1$ excited state of the Eu^{2+} ions.[19] The profile of the excitation spectrum is assigned to the crystal field splitting of 5d level of Eu^{2+} ions. The excited 5d levels are not shielded from the crystal field, giving rise to a marked splitting of the excited level, which makes the excitation spectrum is composed of several excitation peaks. For $Ba(PO_3)_2$: Eu^{2+} phosphor, the excitation peak at 323 nm is the strongest one.

The emission spectra of $Ba_{1-x}(PO_3)_2$: Eu^{2+}_x (x = 0.005, 0.010, 0.020, 0.030, 0.035, 0.040) excited by 323 nm light are shown in Fig. 6 (b). Upon excitation with NUV

light at 323 nm, the sample shows an broad asymmetric intense blue-green emission band with the strongest peak around 445 nm, which ascribes to the electron transition from $4f^6 5d^1$ excited state to $4f^7$ ground state of Eu^{2+}.[20] The emission intensity increases with the increase of Eu^{2+} concentration until a maximum value is reached, and then it decreases due to concentration quenching effect. The inset of Fig. 6 (b) shows the dependence of the emission intensity on the concentration of Eu^{2+}, which suggests that the optimum doping amount of Eu^{2+} is $x = 0.030$. In general, the concentration quenching of luminescence is due to the energy transfer between the activator ions at the high concentrations. In the energy transfer process, the energy is lost at a killer (or quenching) site, resulting in the decrease of luminescence intensity.[21] It is also observed that the emission peaks shift gradually to longer wavelength (from 438 to 450 nm) with increasing the doping concentration of Eu^{2+}, which is consistent with the previous references.[19,22] The inter-atomic distance between two Eu^{2+} ions is expected to become shorter due to the increase of Eu^{2+}-doping concentration, and the interaction is enhanced. The crystal field strength surrounding Eu^{2+} ions is thus increased, leading to the red-shifting of the emission peak.

In addition, the excitation and emission spectra of $Ba_{0.970}(PO_3)_2$: $Eu^{2+}_{0.030}$ and the commercial blue-emitting phosphor BAM are presented in Fig. 7 for comparison. In the range of 310–380 nm, $Ba_{0.970}(PO_3)_2$: $Eu^{2+}_{0.030}$ shows higher excitation intensity than BAM, which is favorable to application in NUV chip based LEDs. Similarly,

$Ba_{0.970}(PO_3)_2$: $Eu^{2+}_{0.030}$ exhibits stronger and broader emission band than BAM upon NUV light excitation.

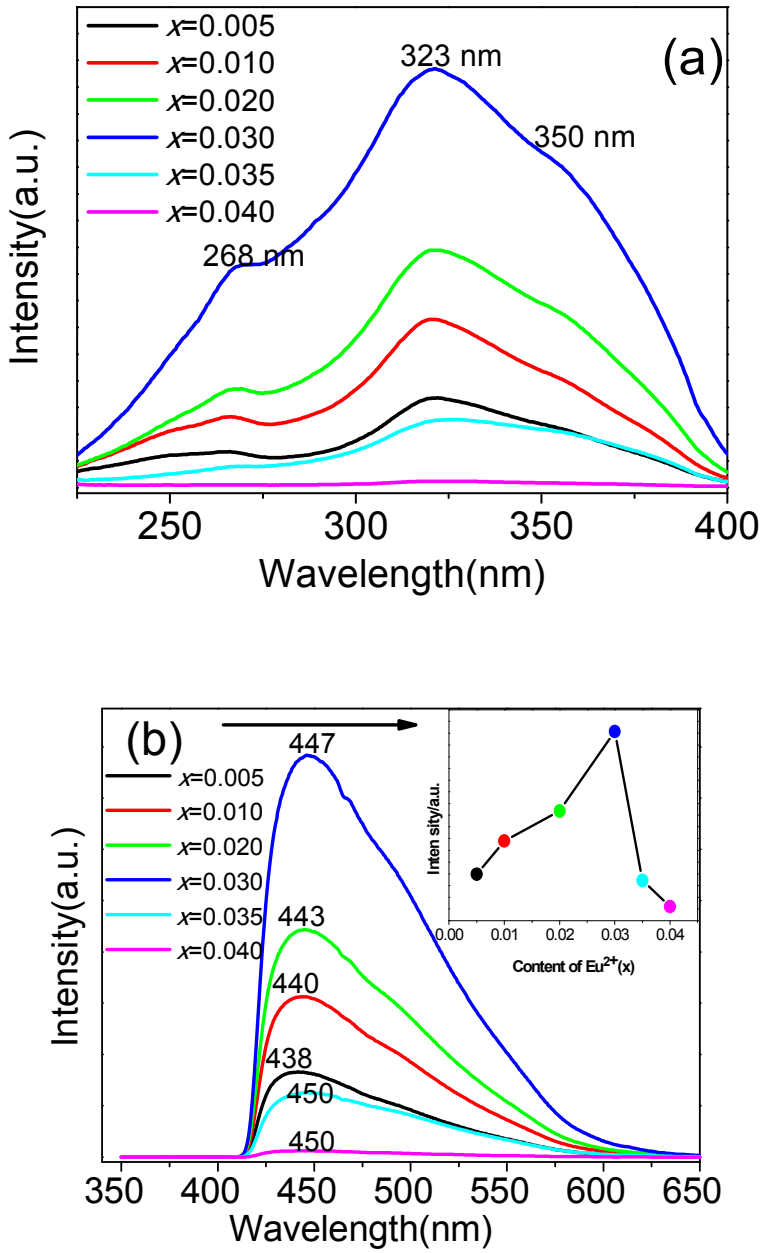

Fig. 6 Photoluminescence spectra of $Ba_{1-x}(PO_3)_2$: Eu^{2+}_x: (a) Excitation spectra (λ_{em} = 445nm) and (b) Emission spectra (λ_{ex} = 323nm). The inset shows emission intensity of $Ba(PO_3)_2$: Eu^{2+} phosphor with different Eu^{2+} concentrations.

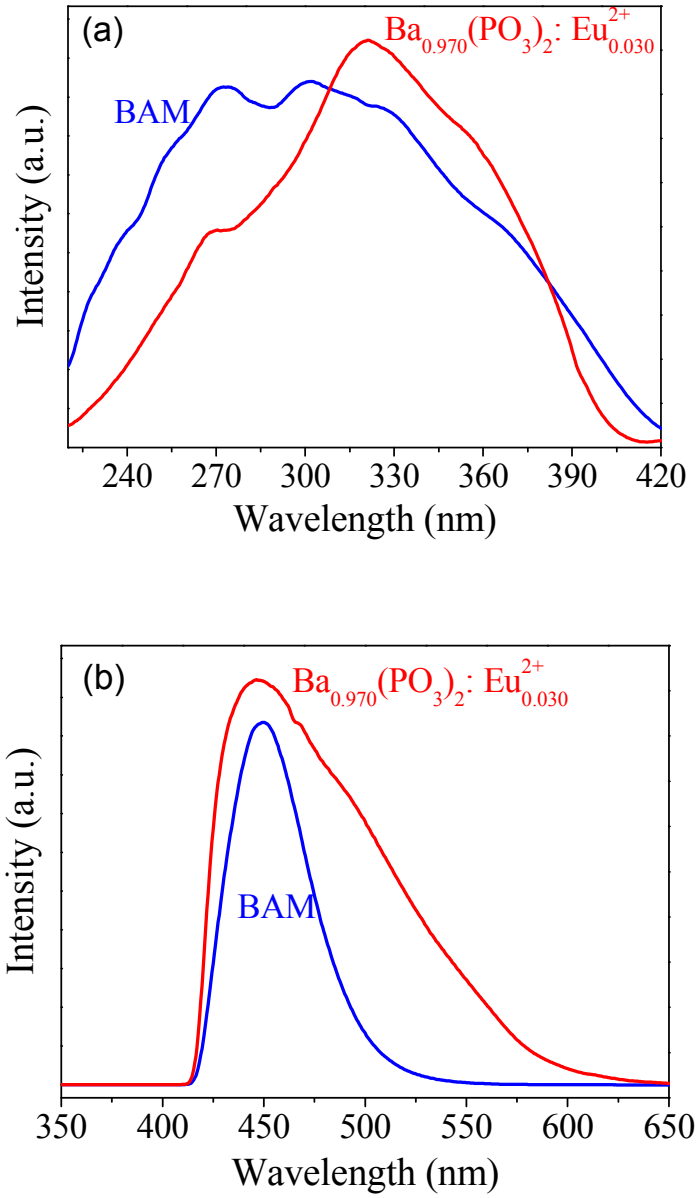

Fig. 7 The excitation (a) and emission (b) spectra of $Ba_{0.970}(PO_3)_2$: $Eu^{2+}_{0.030}$ and BAM.

3.3 Temperature-dependent luminescence properties

The temperature-dependent luminescence of phosphors is an essential parameter, which has great influence on the light output of phosphor used in WLED. Fig. 8 shows temperature-dependent photoluminescence of $Ba_{0.970}(PO_3)_2$: $Eu^{2+}_{0.030}$ phosphor excited at 323 nm in the temperature range of 298–423 K. It can be seen that the

shape, position and intensity of the emission spectra gradually changed with measure temperature increasing from 298 to 423K. The emission integrated intensity of $Ba_{0.970}(PO_3)_2$: $Eu^{2+}_{0.030}$ decreases gradually to 66.5% of the initial value as the temperature increases from 298 to 423K. It is worth note that the emission integrated intensity of $Ba_{0.970}(PO_3)_2$: $Eu^{2+}_{0.030}$ only decreased to 83.6% of the initial value when the temperature increases to 398 K, which is close to the work temperature of LEDs (about 120 ^{o}C). As a comparison, the temperature-dependent luminescence of commercial blue phosphor BAM is also shown in the inset of Fig. 8. The emission integrated intensity of $Ba_{0.970}(PO_3)_2$: $Eu^{2+}_{0.030}$ decreases more slowly than that of BAM. These results suggest that $Ba_{0.970}(PO_3)_2$: $Eu^{2+}_{0.030}$ has higher thermal stability than BAM.

The temperature-dependent emission intensity of $Ba_{0.970}(PO_3)_2$: $Eu^{2+}_{0.030}$ phosphor can be described by a modified Arrhenius equation[23] as:

$$I_T = \frac{I_0}{1 + c\exp(-\frac{E_a}{kT})} \qquad (2)$$

Where I_0 is the initial emission intensity of the phosphor at room temperature, I_T is the emission intensity of the phosphor at different testing temperature, c is a constant and k is the Boltzmann constant (8.617eV). As shown in Fig. 9, the plot of $\ln[(I_0/I)-1]$ *vs* 1000/T could be fitted into a straight line. The Ea value obtained from Fig. 9 was 0.334eV. Compared with the previously reported data,[22,24] $Ba_{0.970}(PO_3)_2$: $Eu^{2+}_{0.030}$ exhibits a relatively high Ea value. The relatively high Ea indicates that the as-prepared phosphor has good thermal stability, which is very beneficial for its application in LED.

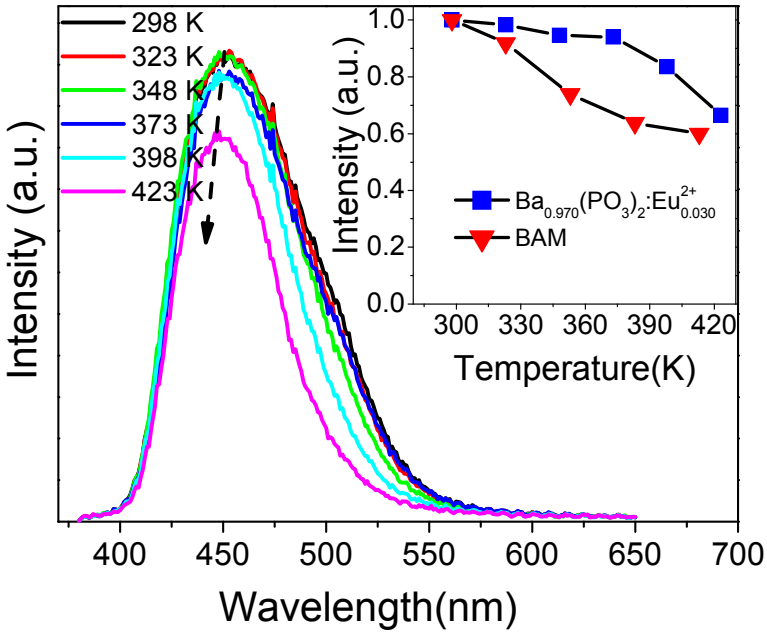

Fig. 8 Emission spectra of $Ba_{0.970}(PO_3)_2$: $Eu^{2+}_{0.030}$ phosphor as a function of temperature (λ_{ex} = 323nm). Inset shows temperature dependent emission intensity of $Ba_{0.970}(PO_3)_2$: $Eu^{2+}_{0.030}$ and commercial blue phosphor BAM.

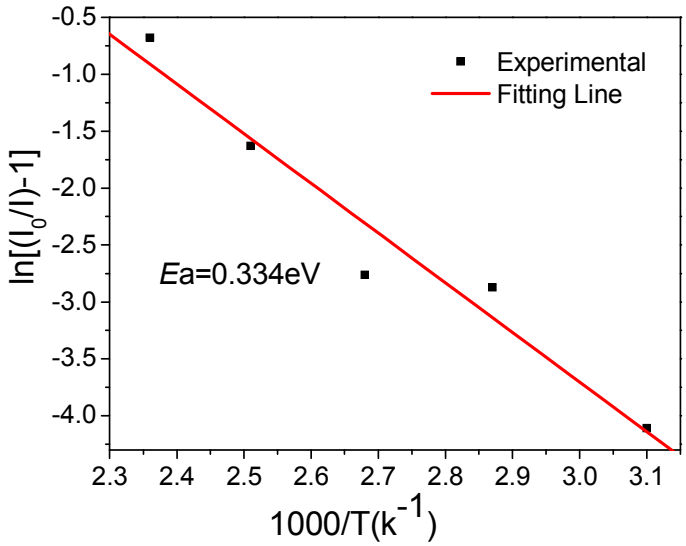

Fig. 9 The Arrhenius fitting of the emission intensity of $Ba_{0.970}(PO_3)_2$: $Eu^{2+}_{0.030}$ phosphor and the calculated activation energy (*E*a) for thermal quenching.

The decrease in emission intensity with increasing temperature can be described by thermal quenching at configuration coordinate diagram (shown in Fig. 10). Through phonon interaction, the excited luminescent center is thermally activated and then thermally released through the crossing point between the excited state and the ground state. This nonradiative transition probability is greatly dependent on the temperature, which leads to the decrease of emission intensity with the increasing temperature. The main mechanism for the temperature quenching of Eu^{2+} luminescence in solids is the thermal excitation of the 5d electron to conduction band states. Probably the 5d electron remains bonded in a Eu^{2+} trapped excited state from which it returns nonradiatively to the Eu^{2+} ground state. The referred activation energy is the energy required to raise the electron from the relaxed excited level into the host lattice conduction band.[25] The high quenching temperature and *E*a for the Eu^{2+} emission in $Ba(PO_3)_2$ indicate that the lowest energy level of the Eu^{2+} $4f^65d^1$ electronic configuration is well isolated from the host lattice conduction band.

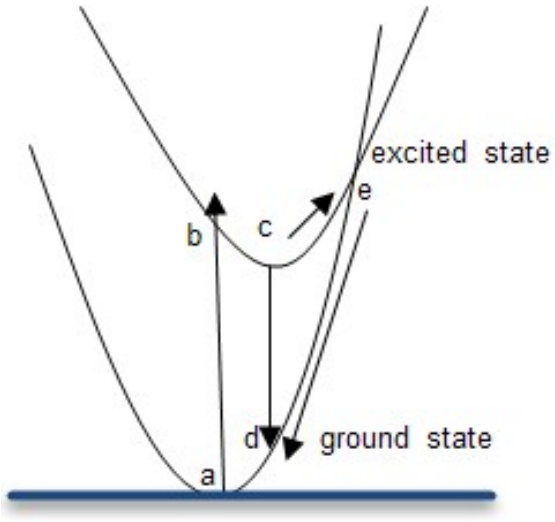

Fig. 10 The schematic configuration coordinate diagram of Eu^{2+} ion

In addition, the maximum emission wavelength of $Ba_{0.970}(PO_3)_2$: $Eu^{2+}_{0.030}$ shows blue shift from 453 to 447 nm with increasing temperature. This phenomenon can be ascribed to the thermal back-transfer over the barrier from the excited states of the low energy emission band to the excited states of the high energy emission band of Eu^{2+} by the assistance of thermally active phonons (given in Fig. 11). At low temperature, the low-energy emission is dominant. As temperature increases, thermally activated phonon-assisted tunneling from the excited states of low-energy emission band to the excited states of high-energy emission band (see Fig. 11) occurs and the electron population of Eu^{2+} in upper vibration level of excited state becomes dominating under phonon-assistant, from which radiative transition happen. Thus, the blue shift is observed with increasing temperature. Just because of this, the profile of emission spectra at high temperature becomes more symmetric gradually (as shown in Fig. 8).

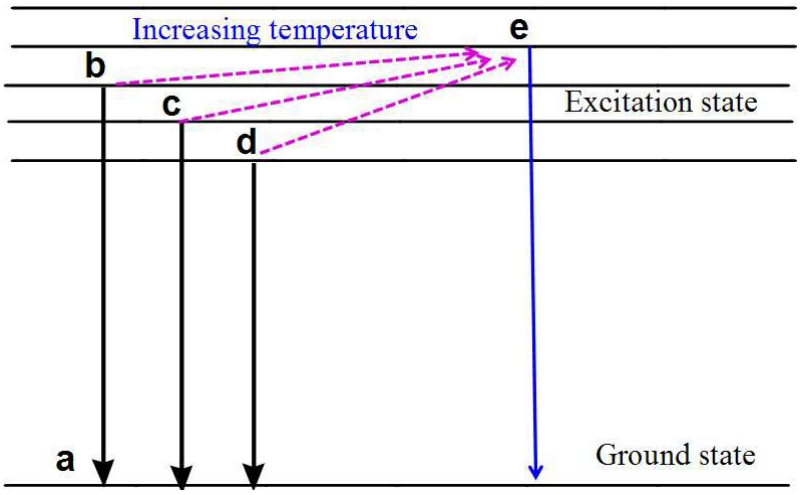

Fig. 11 Schematic diagram of spectrum blue shift at high temperature

3.4 CIE chromaticity coordinates

Fig. 12 shows the Commission International de L'Eclairage (CIE) chromaticity

coordinates calculated from the emission spectrum of $Ba_{1-x}(PO_3)_2$: Eu^{2+}_x (x = 0.005, 0.010, 0.020, 0.030, 0.035) under 323 nm light excitation. As shown in Fig. 12 and Table 2, the CIE chromaticity coordinates shift from (0.162, 0.174) to (0.165, 0.198) as Eu^{2+} concentrations increasing from 0.005 to 0.035. The results indicate that the CIE chromaticity can be varied within a certain range by adjusting the content of Eu^{2+}. The digital image of the $Ba_{0.970}(PO_3)_2$: $Eu^{2+}_{0.030}$ phosphor under NUV light about 365 nm irradiation is also shown in inset of Fig. 12. It can be seen that the sample shows bright blue-green emission.

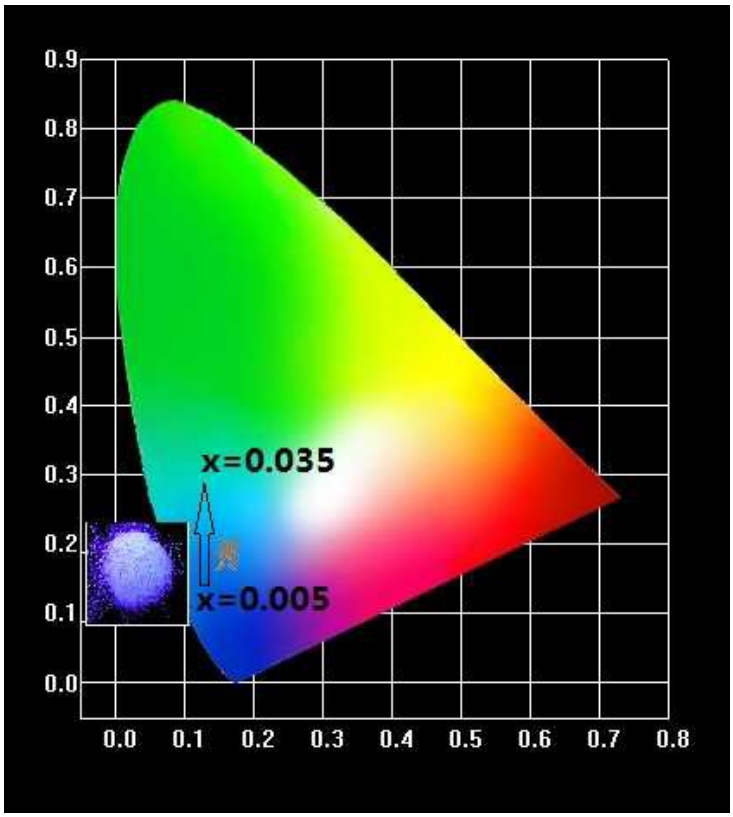

Fig. 12 CIE chromaticity coordinates of $Ba_{1-x}(PO_3)_2$: Eu^{2+}_x (x = 0.005, 0.010, 0.020, 0.030, 0.035) phosphor (λ_{ex}= 323 nm) in the CIE chromaticity diagram.The inset shows a digital image of the $Ba_{0.970}(PO_3)_2$: $Eu^{2+}_{0.030}$ phosphor under 365 nm NUV lamp irradiation.

Table 2. CIE chromaticity coordinates of $Ba_{1-x}(PO_3)_2$: Eu^{2+}_x (x = 0.005, 0.010, 0.020, 0.030, 0.035) phosphors (λ_{ex} = 323 nm).

No.	Composition	CIE（x,y）
1	$Ba_{0.995}(PO_3)_2$: $Eu^{2+}_{0.005}$	(0.162,0.174)
2	$Ba_{0.990}(PO_3)_2$: $Eu^{2+}_{0.010}$	(0.163,0.183)
3	$Ba_{0.980}(PO_3)_2$: $Eu^{2+}_{0.020}$	(0.164,0.188)
4	$Ba_{0.970}(PO_3)_2$: $Eu^{2+}_{0.030}$	(0.164,0.196)
5	$Ba_{0.965}(PO_3)_2$: $Eu^{2+}_{0.035}$	(0.165,0.198)

4. Conclusion

In conclusion, a series of blue-green emitting phosphors $Ba_{1-x}(PO_3)_2$: Eu^{2+}_x (x = 0.005, 0.010, 0.020, 0.030, 0.035) were synthesized by solid-state method at lower temperature of 600 ^oC. The results of XRD and Rietveld refinement indicate that there is only one kind of Ba^{2+} site and Ba^{2+} is substituted by Eu^{2+} in $Ba(PO_3)_2$ host. The photoluminescence excitation spectra are very broad band extending from 200 to 400 nm. Under NUV light excitation, $Ba(PO_3)_2$: Eu^{2+} exhibits strong blue-green emission band peaking at 445 nm. The optimal concentration of Eu^{2+} in $Ba(PO_3)_2$ host is 3.0 mol%. The CIE chromaticity can be varied within a certain range by adjusting the content of Eu^{2+}. The temperature-dependent luminescence shows $Ba_{0.970}(PO_3)_2$: $Eu^{2+}_{0.030}$ have excellent thermal stability. All these results indicate that $Ba(PO_3)_2$: Eu^{2+} phosphor is a promising blue-green emitting phosphor for application in NUV WLEDs.

Acknowledgments

This work was financially supported by the National Natural Science Foundation of the People's Republic of China (No. 51472132), the Natural Science Foundation of Shandong Province (No. ZR2012BQ017), Qingdao Project of Science and Technology (No. 13-1-4-114-jch), the Joint Funds of the National Natural Science Foundation of China and Guangdong Province (No. U1301242), Research Fund for the Doctoral Program of Higher Education of China (RFDP) (No. 20130171130001) and the Guangdong Province project for industrial applications of rare earth materials (2012B09000026).

References

1 M. Krings, G. Montana, R. Dronskowski and C. Wickleder. *Chem. Mater.*, 2011, **23**, 1694–1699.

2 R. J. Xie, N. Hirosaki, M. Mitomo, Y. Yamamoto and T. Suehiro. *J. Phys. Chem. B.*, 2004, **108**, 12027–12031.

3 M. F. Zhang, Y. J. Liang, R. Tang, D. Y. Yu, M. H. Tong, Q. Wang,Y. L. Zhu, X. Y. Wu and G. G. Li, *RSC Adv.*, 2014, **4**, 40626-40637.

4 V. Bachmann, C. Ronda and A. Meijerink. *Chem. Mater.*, 2009, **21**, 2077−2084.

5 W. Chen, and A. Zhou. *J. Phys. Chem. C*, 2012, **116**, 24748-24751.

6 (a)W. R. Liu, C. H. Huang, C. W. Yeh, J. C. Tsai, Y. C. Chiu, Y. T. Yeh and R. S. Liu, *Inorg. Chem.*, 2012, **51**, 9636–9641. (b) C. H. Huang, D. Y. Wang, Y. C.

Chiu, Y. T. Yeh and T. M. Chen, *RSC Adv.*, 2012, **2**, 9130–9134

7 L. Wu, Y. Zhang, M. Y. Gui, P. Z. Lu, L. X. Zhao, S. Tian,Y. F. Kong and J. J. Xu, *J. Mater. Chem.*, 2012, **22**, 6463-6470.

8 X. Chen, P. P. Dai, X. T. Zhang, C. Li, S. Lu, X. L. Wang, Y. Jia, and Y. C. Liu, *Inorg. Chem.*, 2014, **53**, 3441−3448.

9 S. J. Gwak, P. Arunkumar, and W. B. Im, *J. Phys. Chem. C*, 2014, **118**, 2686-2692.

10 X. M. Zhang, F. G. Meng, W. L. Li and H. J Seo, *Ceram. Int.,* 2013, **39**, 8975–8978.

11 T. Z. Zhan, C. N. Xu, H. Yamada, Y. Terasawa, H. Iwase, M. Kawaid and L. Zhang, *RSC Adv.*, 2012, **2**, 328–332.

12 T. G. Kim, T. Y. Kim, J. Y. Kim, S. J. Kim, and S. J. Im, *J. Phys. Chem. C*, 2014, **118**, 12428-12435.

13 T. Suehiro, R. J. Xie and N. Hirosakiet, *Ind. Eng. Chem. Res.*, 2013, **52**, 7453-7456.

14 C.C. Lagos, *J. Electrochem. Soc.: Solid State Sci.Technol.*, 1968, **115**, 1271-1274.

15 P. Dorenbos, *J. Lumin.*, 2003, **104**, 239-260.

16 A. A. Coelho, TOPAS Academic Version 4.1; Coelho Software: Brisbane, Australia, 2007.

17 B. D. Cullity, Element of X-ray Diffraction, 2nd ed., Addison wesley, Reading, MA, 1978.

18 C.C. Wu, K.B. Chen, C.S. Lee, T.M. Chen and B.M. Cheng, *Chem. Mater.*, 2007, **19**, 3278-3285.

19 H.P. Ji, Z.H. Huang, Z.G. Xia, M.S. Molokeev, V.V. Atuchin, M.H. Fang and S.F. Huang, *Inorg. Chem.*, 2014, **53**, 5129-5135.

20 C. H. Huang, D. Y. Wang, Y. C. Chiu, Y. T. Yeh and T. M. Chen, *RSC Adv.*, 2012, **2**, 9130–9134.

21 C. C. Lin, R. S. Liu, Y. S. Tang, and S. F. Huc, *J. Electrochem. Soc.*, 2008, **155**, J248.

22 Y. Zhang, Z. G. Xia and W. W. Wu, *J. Am. Ceram. Soc.*, 2013, **96**, 1043-1046.

23 I. Baginskiy and R. S. Liu, *J. Electrochem. Soc.*,2009, **156**, G29-G32.

24 C. H. Huang, and T. M. Chen, *Inorg. Chem.*, 2011, **50**, 5725-5730.

25 P. Dorenbos, *J.Phys.-Condens. Mat.*, 2005, **17**, 8103-8111.